Design of a fiber cavity ion trap for a high-efficiency and high-rate quantum network node

Xing-Yu Bao[1,2], Jin-Ming Cui[1,2,3] ✉, Ding Fang[1,2], Wei-Bin Chen[1,2], Jian Wang[1,2,3], Yun-Feng Huang[1,2,3], Chuan-Feng Li[1,2,3], and Guang-Can Guo[1,2,3]

[1]CAS Key Laboratory of Quantum Information, University of Science and Technology of China, Hefei 230026, China;
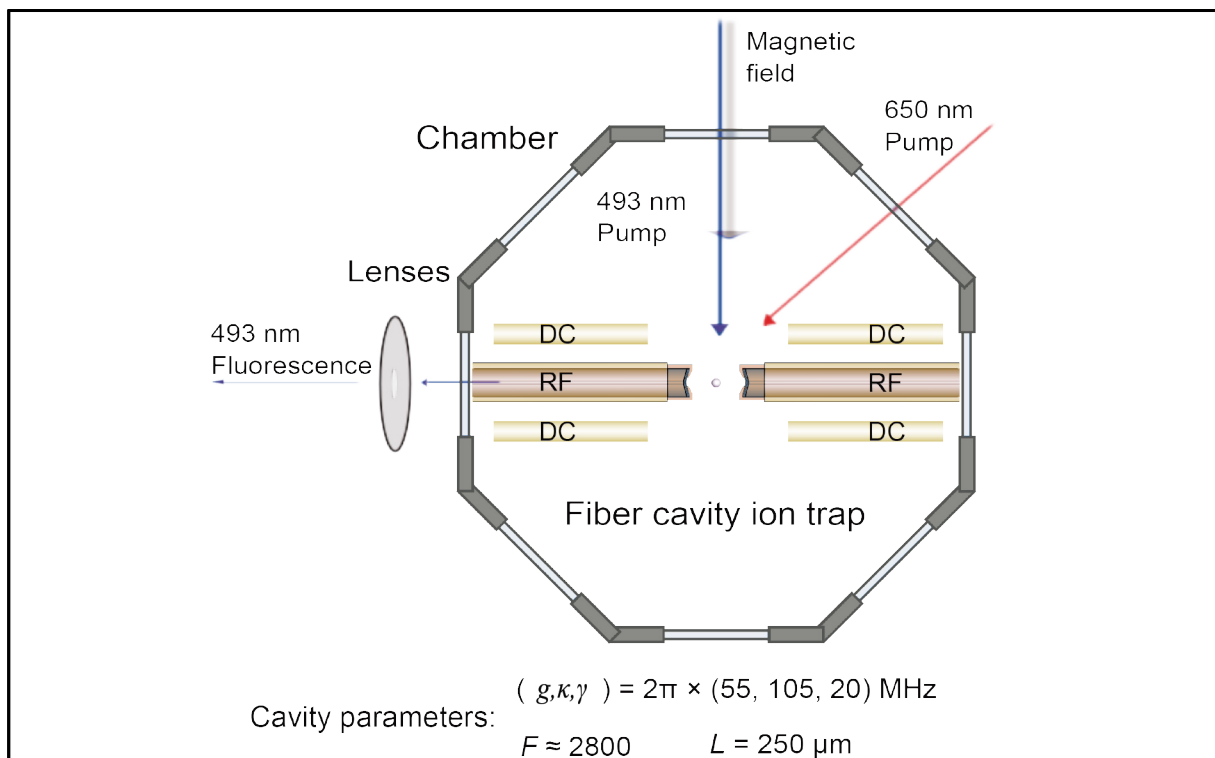[2]CAS Center for Excellence in Quantum Information and Quantum Physics, University of Science and Technology of China, Hefei 230026, China;
[3]Hefei National Laboratory, University of Science and Technology of China, Hefei 230088, China

✉Correspondence: Jin-Ming Cui, E-mail: jmcui@ustc.edu.cn

Graphical abstract

$(g, \kappa, \gamma) = 2\pi \times (55, 105, 20)$ MHz

Cavity parameters:

$F \approx 2800$ $L = 250$ μm

Scheme and parameters of the designed fiber cavity ion trap.

Public summary

■ This work designs a high-efficiency and high-photon-rate quantum node based on a cold trapped ion.

■ The optimized small-mode-volume fiber cavity serves as a resonant cavity to efficiently collect ion fluorescence photons.

■ The end face of the fiber is coated with a metal mask, which can effectively reduce the charging effect of the fiber, contributing to stable ion trapping in the cavity mode.

Design of a fiber cavity ion trap for a high-efficiency and high-rate quantum network node

Xing-Yu Bao[1,2], Jin-Ming Cui[1,2,3] ✉, Ding Fang[1,2], Wei-Bin Chen[1,2], Jian Wang[1,2,3], Yun-Feng Huang[1,2,3], Chuan-Feng Li[1,2,3], and Guang-Can Guo[1,2,3]

[1]CAS Key Laboratory of Quantum Information, University of Science and Technology of China, Hefei 230026, China;

[2]CAS Center for Excellence in Quantum Information and Quantum Physics, University of Science and Technology of China, Hefei 230026, China;

[3]Hefei National Laboratory, University of Science and Technology of China, Hefei 230088, China

✉Correspondence: Jin-Ming Cui, E-mail: jmcui@ustc.edu.cn

Abstract: The main purpose of this paper is to design a novel coupled system of an ion trap and a fiber cavity. This integrated solution is achieved by fabricating a fiber cavity with a metal mask on the side and end faces of the fiber. The fiber cavity with the metal mask can transmit light and electric charges, and the metal mask on the fiber end-face can shield electric charges on the dielectric high-reflection film. This system is designed to trap a single $^{138}Ba^+$ ion and realize coupling of the fiber cavity to the fluorescence at a 493 nm wavelength of $^{138}Ba^+$. To efficiently collect fluorescent photons, we perform a theoretical analysis of the overall system to achieve optimal coupling of each individual part. The cavity length is designed to be 250 μm, and the optimized coupling parameters are $(g, \kappa, \gamma)/2\pi = (55, 105, 20)$ MHz. We also improve the stability and reliability of the system by analyzing the vibration, performance of the ion trap, and thermal stability. The core of the system is composed of materials with similar thermal expansion coefficients to improve thermal stability. The system uses spring connections to isolate vibrations inside and outside the vacuum chamber. We theoretically solve the difficulties of manufacturing the coupled system and have completed the experimental verification of some key technologies. The whole system is expected to be extended into a complex quantum network system to realize quantum computation and communication.

Keywords: ion trap; quantum network; fiber cavity; quantum information; quantum optics

CLC number: O431.2   **Document code:** A

1 Introduction

Quantum nodes, which can act as either a quantum repeater or a terminal quantum node, can be created easily using coupled systems of cold atoms (ions) and optical resonant cavities[1–4]. In this scheme, the ions trapped in the ion trap can be used as carriers for stationary qubits, and the fluorescent photons emitted by the ions can be used as carriers for flying qubits. The optical resonant cavity can be used as a quantum interface for the interaction of qubits between the ions and the photons.

An ion trap was first invented in the 1960s by Paul and Dehmelt[5, 6], who were awarded the Nobel Prize in 1989. This Paul trap uses an alternating electric field to form a saddle potential that alternates at RF frequency, and ions in this alternating potential are eventually trapped in the middle of the saddle. In recent years, scientists have invented various ion-trap structures[7], such as quadrupole traps[8], blade traps[9, 10], and two-dimensional surface traps[11, 12]. Given the current state of development, ion-trap systems are among the best quantum processors. Ion traps can stably trap cold ions with long coherence times for long periods. These ions also provide rich interactions through Coulomb forces, thus enabling various

complex quantum logic gates[3, 9, 13, 14].

Ions trapped in an ion trap are excellent physical materials for constructing quantum networks[1], and one of the keys to employing this structure as a quantum node is to achieve an efficient quantum interface between ions and photons. One of the most straightforward methods is to collect fluorescent photons through a high numerical aperture objective; however, the collection efficiency of this method is limited to less than 50% and is difficult to further improve. Another possible method is to collect fluorescent photons using a parabolic ion trap, which can theoretically reach a collection efficiency close to 1; however, the ions in such ion traps can only receive externally modulated light in the direction of the parabolic plane, which make it difficult to modulate[15, 16]. The most common method is to enhance the collection efficiency by the Purcell effect with a Purcell factor greater than 1. This scheme effectively collects fluorescent photons into the resonant cavity mode, achieving a photon collection efficiency greater than 50%. An optical microcavity with a small mode volume ensures that a single photon generates a strong electric field in the cavity, thus achieving a strong coupling of photons to atoms (ions)[17]. A fiber Fabry-Pérot cavity (FFPC)

developed internationally in the last decade[18], is an ideal optical microcavity in the field of cold atoms (ions). This microcavity has a small mode volume and provides a direct fiber-optic interface, which allows a strong and efficient coupling between single photons and trapped cold atoms.

The long trapping time of the ion trap system provides its critical advantage in developing quantum network research, especially in the case of requiring long storage time of quantum information, such as quantum repeaters. A high-efficiency interface between trapped ion quantum nodes has been realized in a classical optical cavity with a mode volume in the range of mm³[19, 20], and the entangle rate is limited by the coupling factor provided by the millimeter size of the cavity. To further develop the system, minimizing the cavity mode volume is essential, whereas integrating an FFPC into a trapped ion system is a quite realistic approach. The FFPC has been verified as a powerful tool in the neutral cold atom area and has been successfully applied to basic quantum cavity electronic dynamic research[21–23], efficiently preparing entangled multiphoton graph states from a single cold atom[23].

However, integrating an FFPC with an ion trap is still challenging, e.g., Tracy's group tried to place an FFPC in a linear trap[24], but since the fiber end-face is a dielectric material and UV light is required to manipulate the ion energy level, the photoelectric effect when UV light acts on the dielectric material causes the fiber to be charged, which changes the confining potential of the ion trap and eventually leads to the inability of ions to move to the middle of the FFPC. Ballance et al. tried to fabricate an ultraviolet FFPC and an ion trap for strong ion-photon interaction[25], the finesse of the FFPC in the ultraviolet band slowly deteriorates with time in vacuum, and eventually no effective coupling between the cavity and the ions is achieved. Lee et al. designed a micromechanical-based fiber cavity system[26], Takahashi et al. proposed a new single-ion fiber-optic cavity scheme[27], and Teller et al. integrated a fiber cavity into a wheel trap for strong ion-cavity coupling[28]. Although using microcavities to achieve efficient interfaces is one of the feasible ways, it is still very challenging to achieve highly reliable and efficient ion-cavity coupled systems. Experiments in this area have been led by foreign research groups in recent years, and experimental research in this area

is also emerging in China.

2 System design

We design the whole experimental setup according to the schematic diagram shown in Fig. 1. In this setup, the fiber cavity ion trap (FCIT) is placed in the middle of the vacuum chamber. The core parts of the FCIT are the fiber electrodes. These fiber electrodes consist of bare optical fibers with metal-coated surfaces, which are used to transport both charges and photons. Our emitter in this diagram is a single ¹³⁸Ba⁺ ion in the center of the fiber electrodes. The fiber cavity in this trap enhances photon emission on the 493 nm electronic dipole transition. Because the 493 nm wavelength is in the visible light band, it is well suited for transition and modulation.

To stably trap a ¹³⁸Ba⁺ ion and efficiently collect the emitted fluorescent single photons, we constructed an FCIT system. This system is shown in Fig. 2.

The core part of the system is mainly composed of three symmetrical optical fibers with metal-coated surfaces. The optical fiber in the middle is a metal-coated optical fiber that can pass light. The end face of this fiber is properly coated with gold, which can shield the surface charges on the dielectric high-reflection film. Therefore, the fibers in the middle can be used to transmit both light and electric charges. To isolate the external vibration, we use springs to connect the two parts of the stainless steel base, the vacuum chamber is mainly connected with the lower part, and the whole system is assembled on the upper part.

In the following sections, we describe the design requirements of each part in Fig. 2 in detail.

2.1 Fiber electrode

In addition to being used as the electrode of the ion trap, the fiber cavity electrode is also used to form the fiber cavity. The basic steps for fabricating fiber electrodes are as follows:

(i) Use a CO_2 laser to create a pit with the desired radius of curvature on the cut fiber end face.

(ii) Use negative photoresist, through steps such as exposure and development, to create a protective area of appropriate size on the pit.

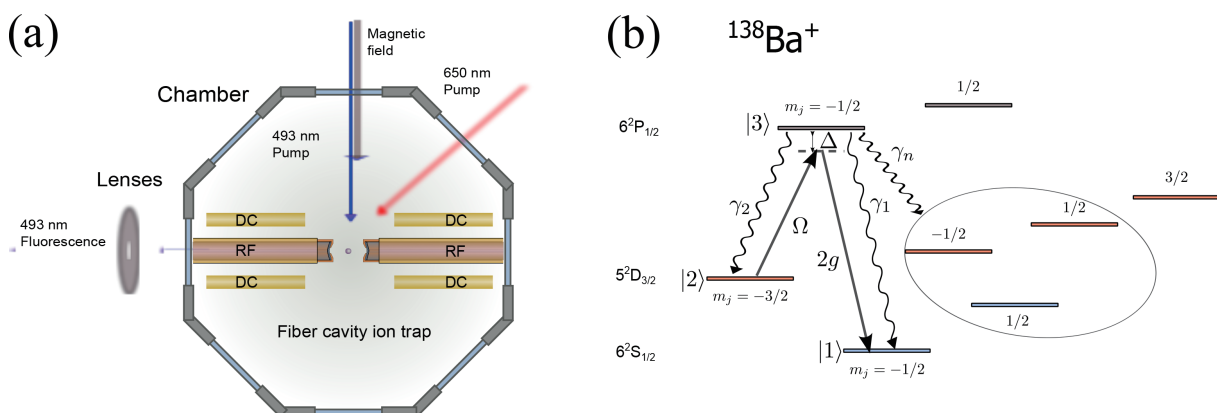(iii) Fabricate a metal layer with a thickness of approximately a dozen nanometers on the entire fiber by evaporation,

Fig. 1. (a) Schematic diagram of the fiber cavity ion trap system. The fiber cavity ion trap is placed in the middle of the vacuum chamber. A single ¹³⁸Ba⁺ ion is trapped in the center. The red and blue lines are the modulation lasers. (b) The basic atomic energy level for photon generation.
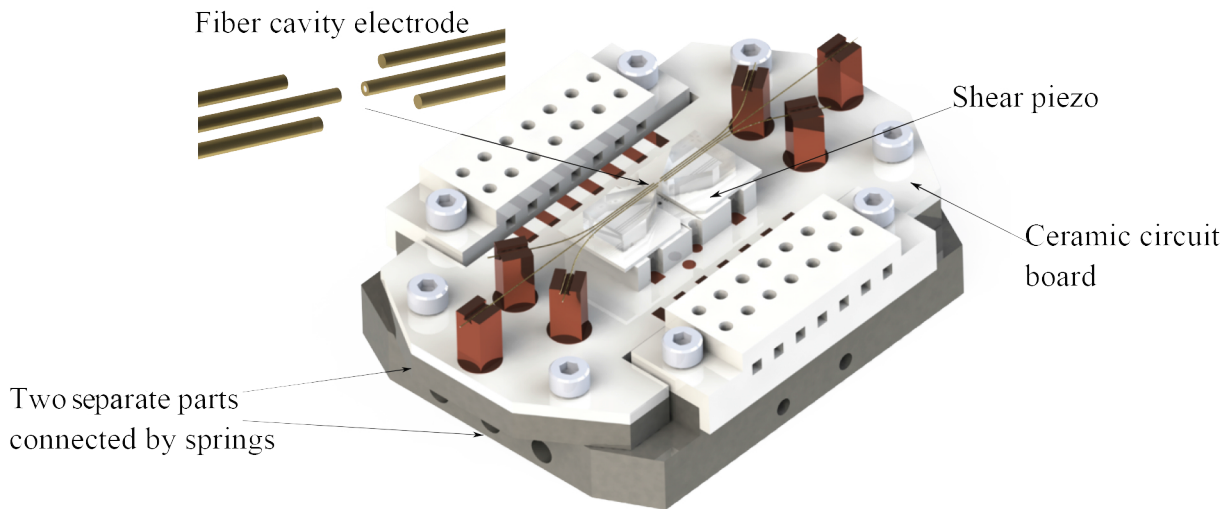
Fig. 2. Diagram of the fiber cavity ion trap system in vacuum. The fiber electrodes are mounted on a fiber mounting base. This system uses a ceramic circuit board to energize the ion trap. The stainless steel base of the device is composed of two spring-connected parts, and the lower part of the stainless steel base is directly connected to the vacuum chamber through grippers.

sputtering, etc.

(ⅳ) Thick the entire metal layer to a few tens of microns by electroplating.

(ⅴ) Use organics such as acetone to remove the photoresist.

The entire flow chart is presented in Fig. 3. The last structure in Fig. 3 is the required fabricated fiber cavity electrode. The central area of the fiber cavity electrode can be used to pass light, and the outer metal layer can be used to pass electricity.

When the cavity surface of the fiber cavity is very close to the location of the ions, the dielectric high-reflection film on the cavity surface is one of the noise sources affecting the ion confinement. The possible effects of the dielectric high-reflection film on ions contain the following aspects: ① The induced electric field that varies with ion motion affects ion cooling[29, 30]. ② The charging effect of the laser on the dielectric high-reflection film changes the electric field[24]. ③ The cavity working for a long time is contaminated with ions, making extra surface charges exist on the surface of the cavity. To eliminate or weaken these effects, as shown in Fig. 3, the fiber surface is wrapped inside a metal layer, and the metal layer is connected to an external power source. By this design, the potential on the dielectric high-reflection film is consistent with the potential of the fiber electrode, i.e., shielding of the charges on the dielectric high-reflection film is achieved. In our evaluation, since the area of the non-conductive region (the region with high resistance) is one order of magnitude smaller, the conductive resistance is one order of magnitude smaller, and the charge is more easily conducted away. In addition, the area receiving light is also one order of magnitude smaller, which makes the area for charging even smaller. Therefore, the charging voltage in our evaluation is reduced by at least two orders of magnitude.

2.2 Ion trap

In our design, the ion trap is mainly composed of six opposing fiber electrodes, as shown in Fig. 1. The two electrodes in the middle propagate the RF electric field, and the four side electrodes propagate the DC electric field. To achieve high light-passing and high Purcell enhancement, the spacing between the RF electrodes is approximately $200-300$ μm, and the DC electrodes are placed at an angle of $30°$ to the center, as shown in Fig. 4. The DC electrodes are grounded by default. In practice, a small voltage can be applied to the DC electrodes to adjust the position of the ions.

All electrodes are placed on borosilicate glass. To install these six fiber electrodes on the same plane and make the opposite fibers coaxial, the fibers are glued in the three scribed grooves of the smoothed high borosilicate glass.

2.3 Support structure

In addition to the core part, the FCIT has a stable support structure to support the core part and a circuit system for powering the fiber electrodes. In Fig. 2, these support structures consist of three parts: base, circuit support plate, and fiber electrode support plate.

The base is made of stainless steel and is fixed to the vacuum chamber with screws and grippers. An external wire pressing device on the base can hold all input wires. These wires are connected to the circuit support plate by conductive elastic wires.

The circuit support plate is constructed of stainless steel and has an aluminum nitride ceramic circuit board screwed onto its surface. The ceramic circuit board implements the circuit system required by the core part. The ceramic circuit board is printed with the power supply circuit, and other conductive separate parts are glued to the ceramic circuit board by conductive silver glue.

The fiber electrode support plate is formed by stacking three parts: high borosilicate glass, shear piezoelectric ceramics, and aluminum nitride ceramic base. Shear piezoelectric ceramics are used for locking the fiber cavity with a travel of approximately a few microns, which will not affect the whole RF and DC electric fields. After these parts are glued together
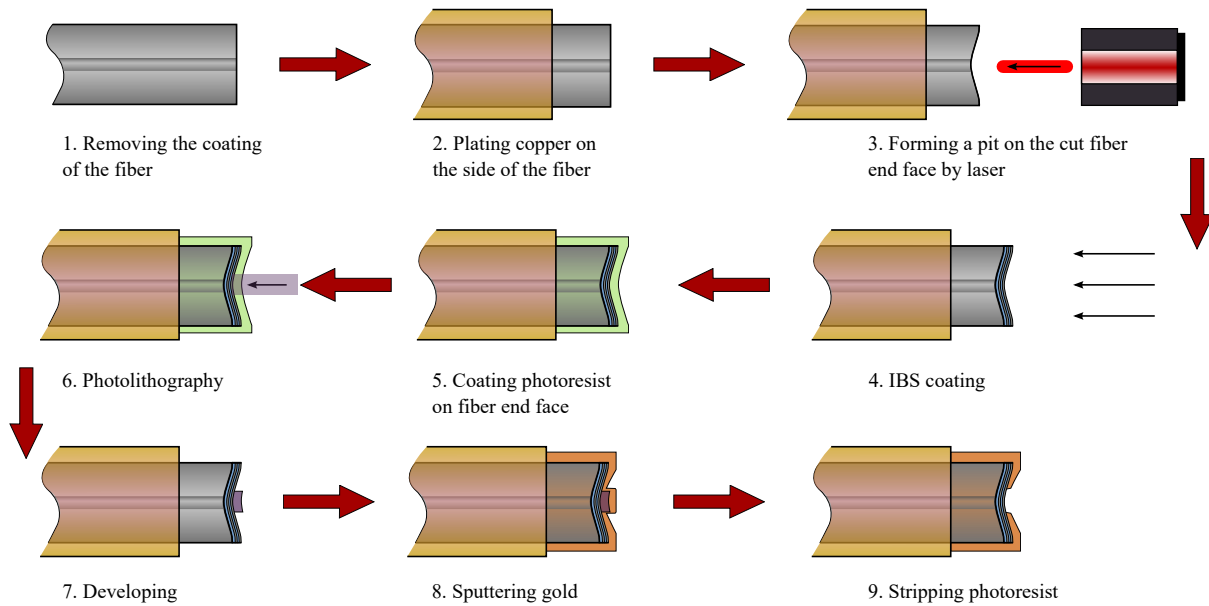
Fig. 3. Flow chart for fabricating fiber electrodes. The cut bare fiber undergoes a complete process to form a central light-permeable electrode structure with a gold layer around the cavity surface to shield the charges from the high-reflection film.
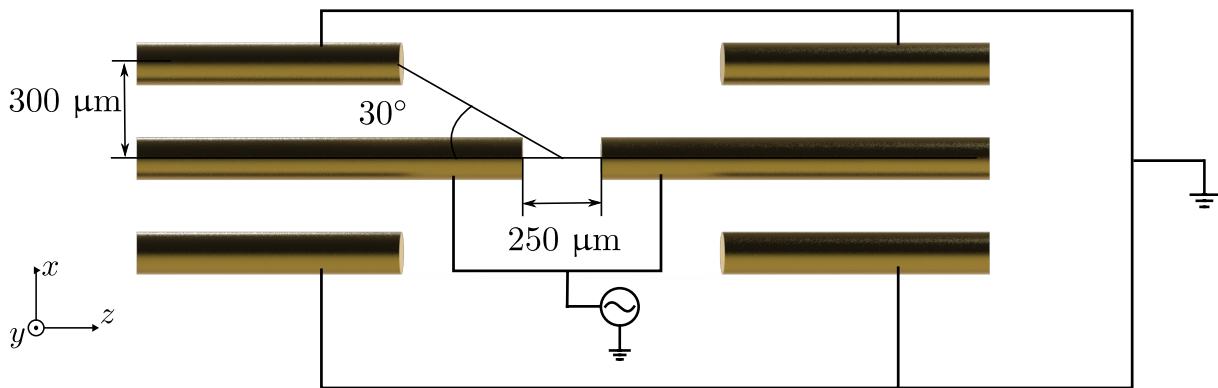

Fig. 4. Arrangement of the fiber electrodes in the system. The four side fiber electrodes are grounded by default, and the middle fiber electrodes are applied with the RF electric field.

with AB glue, a grinding process is used to make the two borosilicate glass surfaces overlap and flat, and a scribing process is used to create fiber electrode mounting grooves on the surface.

3 Simulation and performance

3.1 The optimal fiber cavity

To achieve Purcell enhancement, the structure of the fiber cavity needs to be optimized to match the ion energy level. Referring to Fig. 1 and Fig. 5, the parameters to be considered for the optimal fiber cavity are the fiber type parameters ($n_{f,1}$, $w_{f,1}$, $n_{f,2}$, $w_{f,2}$), the cavity structure parameters (R_1, D_1, R_2, D_2, L) and the coating parameters ($\mathcal{R}_1$, $\mathcal{T}_1$, $\mathcal{L}_1$, $\mathcal{R}_2$, $\mathcal{T}_2$, $\mathcal{L}_2$, which satisfy $\mathcal{R}_i + \mathcal{T}_i + \mathcal{L}_i = 1$, $i = 1, 2$). These parameters are adjusted to maximize the probability of cavity photons emitted by the ions output to the fibers.

Although the smaller the cavity length L, the easier it is to achieve strong coupling, the cavity length L is often limited by the size of the fiber and the overall structure. In this

design, an optical fiber with a cladding diameter of 125 μm is used. Fibers with larger sizes are difficult to use for fabricating fiber electrodes and also limit external laser transmission. In this design, the cavity length is fixed to $L = 250$ μm. Due to the large length of this cavity, a single-sided cavity structure is considered, i.e., photons are emitted from only one side of the fiber cavity. By default, the left fiber is the output side. Since the design is a single-sided cavity structure, there is no need to consider the type of fiber on the right side. For convenience, the fiber types on both sides are set to be the same, i.e., $n_{f,1} = n_{f,2} = n_f$ and $w_{f,1} = w_{f,2} = w_f$. Using the latest coating technology in China, we set the reflectivity $\mathcal{R}_2 = 99.98\%$ at 493 nm for the right fiber and set the coating loss $\mathcal{L}_1 = 30$ ppm for the left fiber. As the reflectivity of the required dielectric film increases, the number of layers of the dielectric in the film will also increase, which will increase the absorption loss. Therefore it is difficult to raise the reflectivity of the dielectric film to an extremely high level. However, for the end face with low reflectivity, the coating loss comes mainly from scattering from the coating surface.

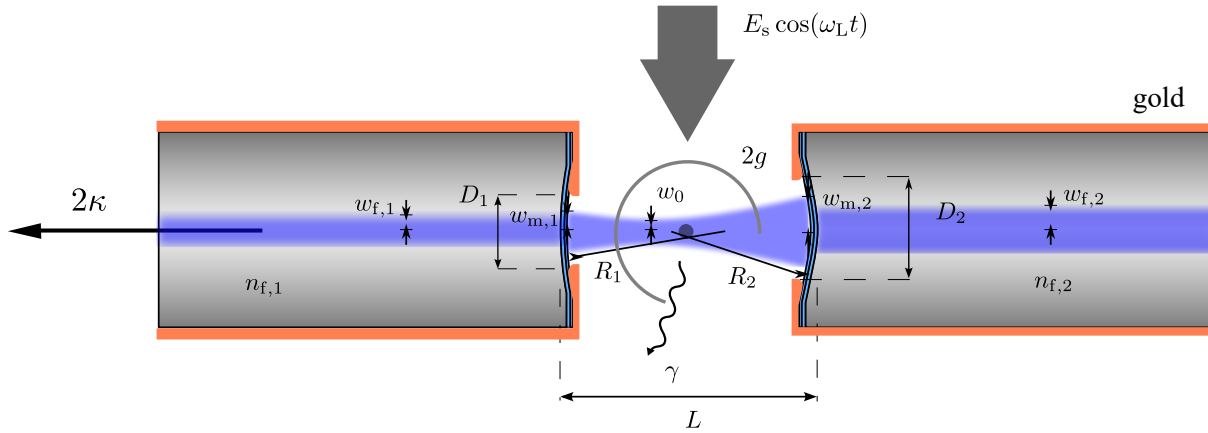The reflectivity $\mathcal{R}_1$ of the left fiber is a very important

Fig. 5. Schematic diagram of the interaction between the fiber cavity and the ion. In the presence of an external electric field $E_s \cos(\omega_L t)$, the single ion interacts with the cavity. In cavity quantum electrodynamics, this interaction can be described using (g, κ, γ). There is only a fundamental mode in the cavity and the distribution is affected by the structure of the cavity. Here, $w_{s,i}$ (s = f, m and i = 1, 2) is the radius of the mode field at each location, w_0 is the radius of the waist, R_i (i = 1, 2) is the radius of curvature (ROC), n_i (i = 1, 2) is the refractive index, and L is the cavity length. At the fiber end face, only the mode field within diameter D_i (i = 1, 2) can be reflected by the fiber.

parameter. $\mathcal{R}_1$ affects the finesse of the fiber cavity and the percentage of transmission in total channels. Using the definition in Supporting information, the percentage of transmission in total channels is given by

$$\eta_t = \frac{1 - \mathcal{L}_1 - \mathcal{R}_1}{2 - \mathcal{R}_2 - \mathcal{R}_1} = \frac{0.99997 - \mathcal{R}_1}{1.0002 - \mathcal{R}_1}. \quad (1)$$

The above equation decreases slowly in the interval $\mathcal{R}_1 < 99.5\%$ and decreases sharply when $\mathcal{R}_1 > 99.5\%$. $\eta_t \approx 0.95$ when $\mathcal{R}_1 = 99.5\%$, but $\eta_t \approx 0.5$ when $\mathcal{R}_1 = 99.97\%$. A too small $\mathcal{R}_1$ leads to a low cavity finesse and thus reduces the coupling of ions to the cavity photons, but a too large $\mathcal{R}_1$ affects the photon output. Therefore, the reflectivity $\mathcal{R}_1$ of the left fiber can be estimated to be in the interval $99.5\% - 99.9\%$.

Considering the flat-concave cavity structure, when the clipping loss of the concave surface is small enough (the cavity diameter satisfies $D_2 \geqslant 5 w_{m,2}$ or the clipping loss is less than 4×10^{-6}), the cavity diameter of the concave surface for a flat-concave cavity structure needs to satisfy

$$D_2 \geqslant 5 \sqrt{\frac{\lambda^2 L^2}{\pi^2 w_f^2} + w_f^2}. \quad (2)$$

$D_2 \geqslant 116$ μm for the S460-HP single-mode fiber, while $D_2 \geqslant 55$ μm for the LMA-10 photonic crystal fiber. Preference is given to the LMA-10 photonic crystal fiber for constructing the fiber cavity because the $40 - 60$ μm diameter cavity surface can be easily fabricated in experiments. The large mode field and single-mode characteristics of LMA-10 photonic crystal fiber facilitate the fabrication of our system.

In addition to the parameters analyzed above, the only parameters that have large tunability are R_1 and R_2, which change the mode of the cavity significantly. When the cavity structure is close to a flat-concave cavity ($R_1 \to \infty$), the optimal mode matching efficiency η_{fc} can be approximated to 1. However, in this case, the ion is not on the waist of the cavity mode, and the single-atom cooperativity parameter C between the ion and the cavity photon is small, which makes the efficiency of photon emission into the cavity η_q small. On the other hand, when the cavity structure is nearly symmetric

($R_1 = R_2$), the ion is on the beam waist of the cavity, and η_q is close to 1, but the mode matching efficiency η_{fc} between the fiber and cavity will be significantly low. The both specific effects are shown in Fig. 6.

The overall efficiency that can be achieved by flat-concave cavities shown in Fig. 6 is generally larger than that achieved by symmetric cavities. However, the ROC of the concave surface of the flat concave cavity is large. Since the CO_2 fiber cavity fabrication technology can easily fabricate fiber cavity surfaces with ROC in the range of $100 - 300$ μm, we prefer to fabricate a concave cavity when the overall efficiency improvement is not significant.

Considering the above constraints, we optimize the parameters of the fiber cavity by numerical optimization methods implemented in Python. The optimized parameters are shown in Table 1. These parameters are achievable using current technology in our laboratory. When this cavity is coupled to a single $^{138}Ba^+$ ion, the optimal cavity can be described $(g, \kappa, \gamma)/2\pi = (55, 105, 20)$ MHz. For this optimal
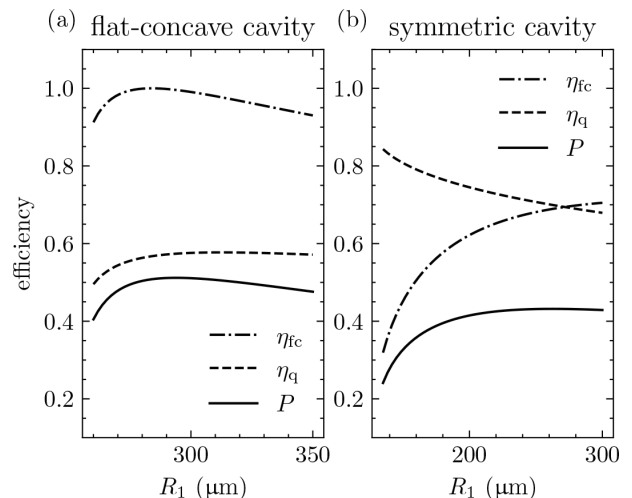

Fig. 6. Variation curves of each coupling with the radius of curvature (ROC) of the left cavity surface R_1 when reflectivity $\mathcal{R}_1 = 99.8\%$, $\mathcal{R}_2 = 99.98\%$, and the type of fiber is LMA-10 photonic crystal fiber. P is the overall efficiency in the figure.

Table 1. Parameters of the optimal fiber cavity in our design, LMA-10 photonic fiber is used for the design.

	Parameter	Value
Cavity length	L	250 μm
Diameter of left cavity surface	D_1	≈ 50 μm
ROC of left cavity surface	R_1	210 μm
Diameter of right cavity surface	D_2	≈ 50 μm
ROC of right cavity surface	R_2	240 μm
Reflectivity of left mirror	$\mathcal{R}_1$	99.80%
Reflectivity of right mirror	$\mathcal{R}_2$	99.98%

fiber cavity, $\mathcal{F} = 2856$ and $C = 1.41$. Therefore, the quantum efficiency is $\eta_q = 0.67$, the matching efficiency is $\eta_{fc} = 0.87$, the transmission efficiency is $\eta_t = 0.90$ and the overall efficiency is $P = 0.53$.

In our design, the overall efficiency is mainly limited by the coating technology. If the finesse can be improved while reducing coating loss, the optimized overall efficiency will be higher under the same conditions. Compared with other research groups in which the finesse of the resonant cavity is larger than 10000[19, 26, 27], our design has a lot of room for improvement. Compared to a collection device consisting of an objective lens with a high numerical aperture, a collection device consisting of a resonant cavity can ensure the collection of photons in opposite directions with significantly higher collection efficiency. In addition, the small-mode fiber cavity has a more significant improvement in overall collection efficiency compared to the resonant cavity implemented with optical lenses, although the fiber cavity introduces an additional mode matching efficiency.

3.2 Performance of the ion trap

The total potential energy in the ion trap is the sum of the RF pseudopotential and the DC potential, which satisfies

$$\Psi_{eff}(\vec{r}) = \frac{1}{4m\Omega^2} \left| \nabla \phi_{RF}(\vec{r}) \right|^2 + \phi_{DC}(\vec{r}), \tag{3}$$

where m represent the mass of a single ion, Ω is the RF frequency, $\phi_{RF}(\vec{r})$ is the electric potential term independent of the RF frequency, and $\phi_{DC}(\vec{r})$ is the electric potential of the DC field. As shown in Fig. 4, in this system, the ions are bound only by the RF electric field. Therefore, only the effect of the $\phi_{RF}(\vec{r})$ term needs to be considered.

In experiments, the RF drive voltage on the fiber electrodes can be set to 100 V, and the drive frequency can be set to $2\pi \times 20$ MHz. At this point, for a single $^{138}Ba^+$ ion, the secular frequencies in the three directions are $(\omega_x, \omega_y, \omega_z) = 2\pi \times (0.84, 0.64, 1.48)$ MHz. The simulated potential energy is shown in Fig. 7. The ions will be trapped in a region with a radius of approximately 20 μm in the center of the fiber electrodes. Although the depth of the ion trap is shallow, it is sufficient to trap a single cold $^{138}Ba^+$ ion. To achieve deeper potential well, the drive voltage can be increased to 200 V without affecting ion trapping. These electrical parameters are consistent with those commonly used in various ion traps, allowing the use of off-the-shelf auxiliary devices such as voltage sources, amplifiers, and helical resonators to be assembled in the FCIT, reducing the additional expense required to purchase and deploy auxiliary devices.

A system composed of a single ion and a resonant cavity is an ideal and easy-to-implement solution for realizing a quantum node. When the number of ions in the ion trap is larger than one, the design of the whole system needs to include the correspondence between photons and individual ions in the resonant cavity, which undoubtedly increases the difficulty of system design and fabrication. Quantum nodes formed by multiple-ion ion traps can be realized by expanding quantum nodes formed by single-ion ion traps. Therefore, the FCIT is mainly used to trap a single $^{138}Ba^+$ ion. However, the potential energy shown in Fig. 7 does not have a flat re-
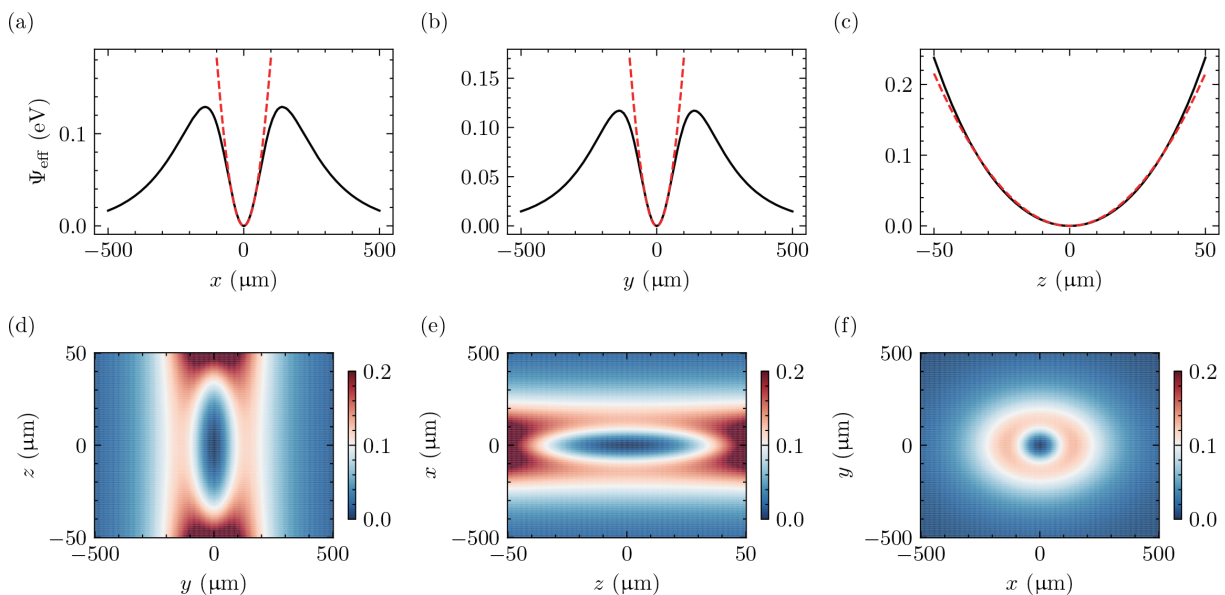

Fig. 7. Simulated potential energy. A drive voltage of 100 V is applied to the RF fiber electrodes. The origin of these figures is the center of the fiber cavity. The curves in (a)–(c) show the potential energy along the x, y, and z directions through the origin, and each red dashed line represents the result of the fit of the quadratic function. The images in (d)–(f) show the potential energy in terms of different cross-section.

gion, which makes the FCIT capture only a single ion with high probability.

3.3 Stability of baking

Since the complete system needs to operate in ultra-high vacuum, the system needs to be baked and evacuated at high temperatures. The higher the baking temperature, the higher the vacuum degree that can be achieved. In this system, the maximum baking temperature is determined by the maximum operating temperature of the shear piezoelectric ceramic. We use the shear piezoelectric ceramic CSAP03 from Noliac, which can reach a maximum operating temperature of 200 ℃.

It is worth noting that, during the heating and cooling process, the fiber cavity may shift due to the different expansion coefficients of different materials, which makes the overall coupling efficiency lower. To solve this problem, a very thin AB glue is needed, and the part connected to the fiber cavity is required to have a similar thermal expansion coefficient.

In our design, the fiber electrodes are glued in the thin grooves of the fiber mounting base shown in Fig. 2. Therefore, the fiber electrode can be considered as a tight fit to the groove, and the offset of the fiber cavity can be regarded as the offset of the relative positions of the two glass grooves. The designed fiber mounting base is composed of high borosilicate glass with $\alpha = 3.3 \times 10^{-6}$ K^{-1}, shear piezoelectric ceramics with $\alpha = 5.5 \times 10^{-6}$ K^{-1}, and aluminum nitride with α ranging from 3.5×10^{-6} to 5.76×10^{-6} K^{-1}, where α is the linear thermal expansion coefficient of each material. And the fiber mounting base has a width of 10 mm and a height of 6.5 mm as shown in Fig. 2. Therefore, by simulating the heating and cooling processes and assuming that the contact surfaces of each material simply slide relative to each other, eventually, in the range of this fiber mounting base, the possible radial offset after heating can be up to 4 μm. This offset size is consistent with the radius of the cavity mode field on the fiber cavity surface and therefore can very significantly reduce the coupling strength between the fiber cavity and the ^{138}Ba$^+$ ion. However, the symmetrically mounted high borosilicate glasses are about 1 mm relative to each other, so that the offset of the fiber cavity is only about 400 nm in this range.

In practice, during the baking process, the materials are held together by the internal stress and hardly slide relative to each other. In order to minimize relative slip, we need to use homogeneous materials and thin uniform strong layer of AB glue. Current manufacturing techniques allow for very small differences in components composed of the same material. Therefore, the main inhomogeneity of the fiber mounting base lies in the difference in gluing thickness between the components. This can be overcome by creating a mounting positioning device that is complementary to the fiber mounting base. By positioning the components in the mounting positioning device and applying pressure, the AB glue can be evenly distributed between the components. In experiments, the bonding strength of the AB glue is sufficient to provide strong internal stresses and eventually a small offset of the fiber cavity is achieved as long as the operation is correct.

3.4 Influence of vibration

Vibration is an important factor affecting the coupling of this system. To isolate the external vibration, we use springs to connect the core part of the FCIT to the external vacuum chamber. This elastic connection is achieved by a two-part stainless steel base, as shown in Fig. 8. The designed FCIT is symmetric, which means that the translational resonant mode does not affect the coupling of this system. As shown in Fig. 8, the stainless steel base uses a total of ten springs to achieve the connection, and the springs in the same direction have the same properties. The side springs can be mounted using spring mounting holes and secured using screws.

To evaluate the vibration of this system, we mainly use COMSOL to analyze the modes of this system at resonance. In our evaluation, the core parts mounted on the upper half of the stainless steel base are seen as a whole, i.e., the relative displacement of the contact surfaces of each part is the same. The core parts are in contact with the vacuum chamber only at the individual spring connections. The stiffness coefficient of all springs is set to be $k = 2400$ N/m, which can be easily implemented in experiments. Based on this model, we analyzed the resonant frequencies and modes of the system using COMSOL.

The basic resonant modes of this upper part in Fig. 8 are shown in Fig. 9, and the resonant frequencies of this part are between 22 Hz and 39 Hz. Since it is very difficult to install damping devices in vacuum, the damping of the system in vacuum is mainly provided by the springs themselves. The springs made of stainless steel in the system have a damping factor of about 0.003. The magnitude of the transfer function of the spring system in any single direction is given by

$$|H(\beta)| = \frac{1}{\sqrt{(1-\beta^2)^2 + 4\zeta^2\beta^2}}, \tag{4}$$

where β is the ratio of the excitation frequency to the undamped intrinsic frequency in a single direction, and ζ is the damping factor. Therefore, this spring system is able to suppress high frequency vibrations above 100 Hz. The typical resonant frequency of the CSAP03 piezoelectric ceramics used in the system for locking the fiber cavity can reach several kilohertz and higher. Therefore, the resonant frequencies of the spring system are in the operating frequency range of the piezoelectric ceramics. We use piezoelectric ceramics to build a servo to actively suppress vibrations at frequencies below 100 Hz.

4 Discussion

This designed coupled system can be used as a quantum node in a quantum network. This design overcomes the difficult problem of assembling the fiber cavity with the ion trap and solves the problem of shielding the charges in the dielectric high-reflection film on the end face of the fiber cavity[24–27, 31]. After our initial validation, our scheme can be easily implemented in the laboratory. The remarkable feature of this designed system is the coupling between the ion trap and the fiber cavity using electrodes made of optical fibers. This reduces the complexity of the system and makes it easy to manufacture in volume. Multiple such systems can be connected using optical fibers, and such extended system can be used in complex quantum networks.

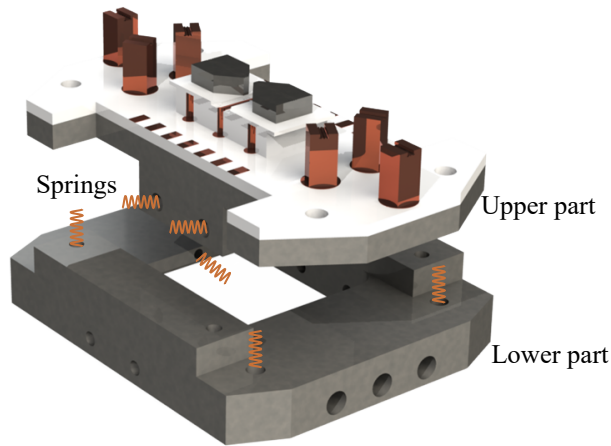In this paper, we adopt a single ^{138}Ba$^+$ as the trapped ion.

Fig. 8. Schematic diagram of the connection of the stainless steel base. The figure shows the spring arrangement as seen from the side. The stainless steel base uses a total of ten springs, four of which are used to achieve the connection in the vertical direction, and the remaining six springs are used to achieve the connection in the side.

The transitions $6^2P_{1/2} \leftrightarrow 6^2S_{1/2}$ and $6^2P_{1/2} \leftrightarrow 5^2D_{3/2}$ in $^{138}Ba^+$ can be used to achieve deterministic photon emission. The corresponding transition wavelengths are 493 nm and 650 nm, both in the visible wavelength band, which can pass through single-mode fibers with low loss. However, the spontaneous radiation rate γ of $^{138}Ba^+$ is relatively large, which corresponds to a relatively short lifetime. Therefore, a large coupling factor, g, is required to achieve deterministic photon emission, which is difficult in a resonant cavity composed of optical lenses. If an ion with a smaller spontaneous radiation rate γ, such as Ca^+, is used, the overall coupling efficiency corresponding to the same designed coupled system will increase accordingly.

5   Conclusions

We design and investigate an ion-cavity coupled system that can be implemented using current technology. The ion-cavity is implemented by fabricating a metal layer on the surface and end face of the fiber. The fabricated fiber electrodes are mounted on a fiber mounting base composed of materials with similar coefficients of linear thermal expansion and are connected to the vacuum chamber using springs. The resonant frequencies are approximately a few tens of hertz. In addition, the cavity length of the fiber cavity is set to approximately 250 μm, and the cavity structure is optimized to form a strong trapping potential for ion-cavity coupling. This overall coupling efficiency after optimization is about 53% for a single $^{138}Ba^+$ ion, mainly limited by the recent coating technology. This design constitutes a promising approach to constructing scalable quantum networks.

Supporting information

The supporting information for this article can be found online at https://doi.org/10.52396/JUSTC-2023-0005.The supporting information includes the theoretical proof of the coupling between an ion and the fiber cavity.

Acknowledgements

22. 1 Hz

25. 1 Hz
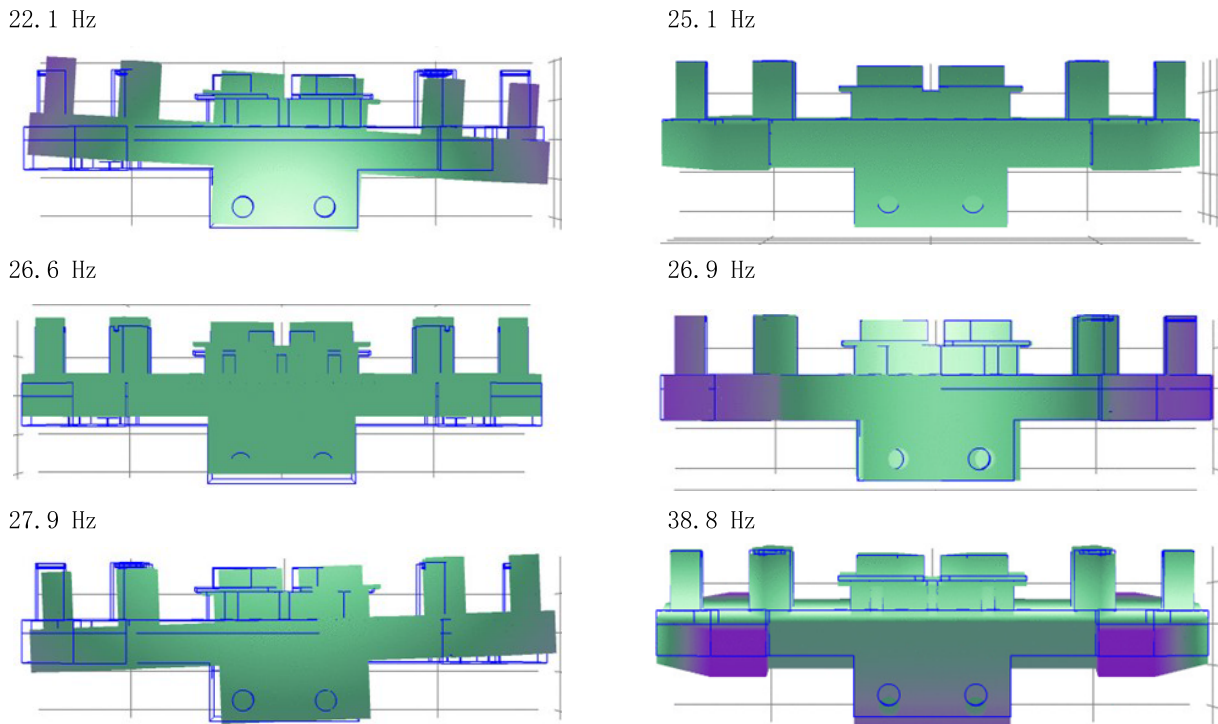
26. 6 Hz

26. 9 Hz

27. 9 Hz

38. 8 Hz

Fig. 9. Simulated resonant modes of the upper part of the system. The solid blue lines in the figure are the original position of the upper part. The darker the color, the greater the displacement of the upper part.

Conflict of interest

The authors declare that they have no conflict of interest.

Biographies

Xing-Yu Bao   received his master's degree in Physics from the University of Science and Technology of China in 2023. His research mainly focuses on ion trap and quantum computing.

Jin-Ming Cui   works as an Associate Researcher in the University of Science and Technology of China. He got his B.S. degree and Ph.D. degree from USTC in 2008 and 2013, respectively. During his Ph.D.'s study, he focused on experiment works with optical micro-cavities and NV centers. Now his major research focuses on quantum information based on trapped ion system, including quantum simulation, quantum computation, quantum network, and fiber Fabry-Perot microcavity.

References

[1] Duan L M, Monroe C. *Colloquium*: Quantum networks with trapped ions. *Reviews of Modern Physics,* **2010**, *82*: 1209–1224.

[2] Ritter S, Nölleke C, Hahn C, et al. An elementary quantum network of single atoms in optical cavities. *Nature,* **2012**, *484*: 195–200.

[3] Reiserer A, Kalb N, Rempe G, et al. A quantum gate between a flying optical photon and a single trapped atom. *Nature,* **2014**, *508*: 237–240.

[4] Uphoff M, Brekenfeld M, Rempe G, et al. An integrated quantum repeater at telecom wavelength with single atoms in optical fiber cavities. *Applied Physics B,* **2016**, *122*: 46.

[5] Paul W, Raether M. Das elektrische massenfilter. *Zeitschrift Für Physik,* **1955**, *140*: 262–273.

[6] Paul W. Electromagnetic traps for charged and neutral particles. *Reviews of Modern Physics,* **1990**, *62*: 531–540.

[7] Wang C X, He R, Li R R, et al. Advances in the study of ion trap structures in quantum computation and simulation. *Acta Physica Sinica,* **2022**, *71*: 133701.

[8] Prestage J D, Dick G J, Maleki L. New ion trap for frequency standard applications. *Journal of Applied Physics,* **1989**, *66*: 1013–1017.

[9] Schmidt-Kaler F, Häffner H, Gulde S, et al. How to realize a universal quantum gate with trapped ions. *Applied Physics B,* **2003**, *77*: 789–796.

[10] He R, Cui J M, Li R R, et al. An ion trap apparatus with high optical access in multiple directions. *Review of Scientific Instruments,* **2021**, *92*: 073201.

[11] Chiaverini J, Blakestad R B, Britton J, et al. Surface-electrode architecture for ion-trap quantum information processing. *Quantum Information and Computation,* **2005**, *5*: 419–439.

[12] David Romaszko Z, Hong S, Siegele M, et al. Engineering of microfabricated ion traps and integration of advanced on-chip features. *Nature Reviews Physics,* **2020**, *2*: 285–299.

[13] Leibfried D, Blatt R, Monroe C, et al. Quantum dynamics of single trapped ions. *Reviews of Modern Physics,* **2003**, *75*: 281–324.

[14] Mehta K K, Zhang C, Malinowski M, et al. Integrated optical multi-ion quantum logic. *Nature,* **2020**, *586*: 533–537.

[15] Chou C K, Auchter C, Lilieholm J, et al. Note: Single ion imaging and fluorescence collection with a parabolic mirror trap. *Review of Scientific Instruments,* **2017**, *88*: 086101.

[16] Wang Z, Wang B R, Ma Q L, et al. Design of a novel monolithic parabolic-mirror ion-trap to precisely align the RF null point with the optical focus. arXiv: 2004.08845, **2020**.

[17] Law C K, Kimble H J. Deterministic generation of a bit-stream of single-photon pulses. *Journal of Modern Optics,* **1997**, *44*: 2067–2074.

[18] Hunger D, Steinmetz T, Colombe Y, et al. A fiber Fabry-Perot cavity with high finesse. *New Journal of Physics,* **2010**, *12*: 065038.

[19] Schupp J, Krcmarsky V, Krutyanskiy V, et al. Interface between trapped-ion qubits and traveling photons with close-to-optimal efficiency. *PRX Quantum,* **2021**, *2*: 020331.

[20] Krutyanskiy V, Galli M, Krcmarsky V, et al. Entanglement of trapped-ion qubits separated by 230 meters. *Physical Review Letters,* **2023**, *130*: 050803.

[21] Wilk T, Webster S C, Kuhn A, et al. Single-atom single-photon quantum interface. *Science,* **2007**, *317*: 488–490.

[22] Daiss S, Langenfeld S, Welte S, et al. A quantum-logic gate between distant quantum-network modules. *Science,* **2021**, *371*: 614–617.

[23] Thomas P, Ruscio L, Morin O, et al. Efficient generation of entangled multiphoton graph states from a single atom. *Nature,* **2022**, *608*: 677–681.

[24] Brandstätter B, McClung A, Schüppert K, et al. Integrated fiber-mirror ion trap for strong ion-cavity coupling. *The Review of Scientific Instruments,* **2013**, *84*: 123104.

[25] Ballance T G, Meyer H M, Kobel P, et al. Cavity-induced backaction in Purcell-enhanced photon emission of a single ion in an ultraviolet fiber cavity. *Physical Review A,* **2017**, *95*: 033812.

[26] Lee M, Lee M, Hong S, et al. Microelectromechanical-system-based design of a high-finesse fiber cavity integrated with an ion trap. *Physical Review Applied,* **2019**, *12*: 044052.

[27] Takahashi H, Kassa E, Christoforou C, et al. Strong coupling of a single ion to an optical cavity. *Physical Review Letters,* **2020**, *124*: 013602.

[28] Teller M, Messerer V, Schüppert K, et al. Integrating a fiber cavity into a wheel trap for strong ion-cavity coupling. *AVS Quantum Science,* **2023**, *5*: 012001.

[29] Kumph M, Henkel C, Rabl P, et al. Electric-field noise above a thin dielectric layer on metal electrodes. *New Journal of Physics,* **2016**, *18*: 023020.

[30] Teller M, Fioretto D A, Holz P C, et al. Heating of a trapped ion induced by dielectric materials. *Physical Review Letters,* **2021**, *126*: 230505.

[31] Sterk J D, Luo L, Manning T A, et al. Photon collection from a trapped ion-cavity system. *Physical Review A,* **2012**, *85*: 062308.